Near-Infrared Luminescent Hybrid Materials Doped with Lanthanide (Ln) Complexes (Ln = Nd, Yb) and Their Possible Laser Application

Li-Ning Sun,[†,‡] Hong-Jie Zhang,*[,†] Qing-Guo Meng,[†] Feng-Yi Liu,[†] Lian-She Fu,[†] Chun-Yun Peng,[†,‡] Jiang-Bo Yu,[†,‡] Guo-Li Zheng,[†,‡] and Shu-Bin Wang[†]

Key Laboratory of Rare Earth Chemistry and Physics, Changchun Institute of Applied Chemistry, Chinese Academy of Sciences, Changchun 130022, People's Republic of China, and Graduate School of the Chinese Academy of Sciences, People's Republic of China

Received: November 29, 2004; In Final Form: January 31, 2005

The crystal structures of ternary $Ln(DBM)_3$phen complexes (DBM = dibenzoylmethane, phen = 1,10-phenanthroline, and Ln = Nd, Yb) and their in situ syntheses via the sol−gel process are reported. The properties of the $Ln(DBM)_3$phen complexes and their corresponding Ln^{3+}/DBM/phen-co-doped luminescent hybrid gels obtained via an in situ method (Ln−D−P gel) have been studied. The results reveal that the lanthanide complexes are successfully in situ synthesized in the corresponding Ln−D−P gels. Both $Ln(DBM)_3$phen complexes and Ln−D−P gels display sensitized near-infrared (NIR) luminescence upon excitation at the maximum absorption of the ligands, which contributes to the efficient energy transfer from the ligands to the Ln^{3+} ions (Ln = Nd, Yb), an antenna effect. The radiative properties of the Nd^{3+} ion in a Nd−D−P gel are discussed using Judd−Ofelt analysis, which indicates that the $^4F_{3/2} \rightarrow {}^4I_{11/2}$ transition of the Nd^{3+} ion in the Nd−D−P gel can be considered as a possible laser transition.

1. Introduction

The trivalent lanthanide ions have been known for their unique optical properties such as line-like emission spectra and high-luminescence quantum efficiency.[1] Historically, detailed research has been almost exclusively devoted to europium and terbium luminescence.[2] Recently, much attention has been paid to near-infrared (NIR) luminescence of lanthanide ions, which are emissive in the near-infrared region of the spectrum (800−1700 nm), particularly neodymium[3] and ytterbium.[4] There are two particular driving forces for this recent interest in NIR luminescence. First, Nd-containing systems have been regarded as the most popular infrared luminescent materials for application in laser systems (the basis of the common 1064 nm laser).[5] Second, the relative transparency of human tissue at approximately 1000 nm suggests that in vivo luminescent probes operating at this wavelength (Yb-based emission) could have diagnostic value.[6] Therefore, developing strongly luminescent Nd^{III} and Yb^{III} centers in these systems has been an attractive target.

Since Weissman discovered that in the lanthanide complex the excitation may be accomplished, under suitable conditions, through light absorption by other constituents of the rare earth compound, with subsequent transfer of energy to the rare earth ion,[7] numerous lanthanide complexes have been studied in detail.[8] The formation of complex between a lanthanide ion and a certain organic ligand has a double beneficial effect on both protecting metal ions from vibrational coupling and increasing the light absorption cross section by "antenna effects".[9] The energy transfer from organic chromophores to lanthanide ions provides an effective way to excite the long-lived, sharply spiked emission. Provided that most of the excitation energy is transferred from the antenna chromophore to the central luminescent lanthanide ion, this process is much more effective than direct excitation, since the absorption coefficients of organic chromophores are many orders of magnitude larger (typically 3−5) than the intrinsically low molar absorption coefficients of trivalent lanthanide ions.[10]

However, due to poor photostability and thermal stability, these light-emitting compounds have to be embedded into a matrix for practical applications. Sol−gel hybrid materials composed of both inorganic and organic components enable both inorganic and organic dopants to be incorporated with relatively high stability.[11] Therefore, sol−gel hybrid materials are potential candidates for practical applications. The sol−gel glasses doped with lanthanide complexes are transparent and have good mechanical properties, except these materials have some drawbacks, such as the low solubility of lanthanide complexes in the sol−gel matrix at the low pH needed for the hydrolysis reaction.[12] Qian et al.[13] reported the in situ synthesis technique and succeeded in doping lanthanide complexes into sol−gel glass at a molecular level and with a high concentration by using the technique. Therefore, in this work, the in situ approach was selected to synthesize the neodymium and ytterbium complexes in sol−gel materials, respectively.

In this paper, we report the structures of $Ln(DBM)_3$phen complexes (DBM = dibenzoylmethane, phen = 1,10-phenanthroline, and Ln = Nd, Yb) and the syntheses of homogeneous transparent hybrid gels containing the corresponding lanthanide complexes via the in situ approach (Ln−D−P gel). At the same time, the properties of the $Ln(DBM)_3$phen complexes and Ln−D−P gels were investigated by FT-IR, diffuse reflectance (DR), and luminescence spectra. A model of the indirect excitation mechanism is suggested. Accordingly, the energy transfer from the ligands to the central Ln^{3+} ions (Ln = Nd, Yb) as well as the NIR luminescence of the Ln^{3+} ions is discussed. The optical

* Author to whom correspondence should be addressed. Phone: +86-431-5262127. Fax: +86-431-5698041. E-mail: hongjie@ns.ciac.jl.cn.

† Changchun Institute of Applied Chemistry, Chinese Academy of Sciences.

‡ Graduate School of the Chinese Academy of Sciences.

10.1021/jp044591h CCC: $30.25
Published on Web 03/08/2005

properties of the Nd^{3+} ion in the Nd−D−P gel are discussed using the theory developed by Judd and Ofelt.[14]

2. Experimental Section

2.1. Synthesis of the Ln(DBM)$_3$phen (Ln = Nd, Yb) Complex. The Ln(DBM)$_3$phen complex was prepared according to the following process. Lanthanide chloride was obtained by dissolution of Ln_2O_3 in hydrochloric acid. DBM and phen in a stoichiometric molar ratio were dissolved in a suitable volume of anhydrous ethanol. Then, an appropriate amount of 1 M sodium hydroxide solution was added dropwise to the solution to adjust the pH value to approximately 7. A stoichiometric amount of lanthanide chloride ethanol solution was then added dropwise to the solution under stirring. The molar ratio of Ln^{3+}/DBM/phen was 1:3:1. The precipitates were collected after filtration and dried at 70 °C under vacuum overnight. The lanthanide complex was recrystallized from an ethanol/acetone mixture. A blue single crystal for Nd(DBM)$_3$phen·0.5(C_2H_5-OH) and a yellow single crystal for Yb(DBM)$_3$phen were obtained by slow evaporation from the mixed mother liquor at room temperature (RT), respectively.

Elemental Analysis. For Nd(DBM)$_3$phen·0.5(C_2H_5OH), calculated: C, 68.48%; H, 4.36%; N, 2.75%. Found: C, 68.44%; H, 4.46%; N, 2.80%. For Yb(DBM)$_3$phen, calculated: C, 66.92%; H, 4.04%; N, 2.74%. Found: C, 66.98%; H, 4.12%; N, 2.79%.

2.2. Single-Crystal X-ray Diffraction Study. X-ray data for the selected crystal mounted on a glass fiber were collected on a CCD area detector with graphite-monochromated Mo Kα radiation. Reflections were collected with a Bruker SMART APEX detector and processed with SAINT from Bruker. Data were corrected for Lorentz and polarization effects. The structure was solved by direct methods and expanded using Fourier techniques. For Nd(DBM)$_3$phen·0.5(C_2H_5OH), the non-hydrogen atoms except O(7), C(58), and C(59) were refined anisotropically. Hydrogen atoms on the ethanol of Nd(DBM)$_3$phen·0.5(C_2H_5OH) were not included, and other hydrogen atoms of Nd(DBM)$_3$phen·0.5(C_2H_5OH) and Yb(DBM)$_3$phen were included using a riding model. All calculations were performed using the Bruker SHELXTL crystallographic software package. Data for the two complexes have been deposited at the Cambridge Crystallographic Database Center.[15a]

2.3. In situ synthesis of a Lanthanide complex via a Sol−Gel Process (Ln−D−P gel, Ln = Nd, Yb). The molar ratio of tetraethoxysilane (TEOS)/ethanol/deionized water (acidified with HCl) in starting solution was 1:4:4. The resulting clear sol with a pH value of about 2.5 was stirred for 2 h. Then, DBM, phen, and $LnCl_3$ ethanol solution were introduced into the starting solution consecutively. The molar ratio of Ln^{3+}/DBM/phen was 1:3:1, and the concentration of the Ln^{3+} ion is Ln^{3+}/Si = 1 mol %. The mixed solution was stirred for several hours at RT to ensure homogeneous mixing and complete hydrolysis, and then placed in a sealed plastic container. The precursor solution converted to wet gel after several days of gelation at 40 °C and then was continuously dried to obtain a transparent monolithic gel. The lanthanide complexes were supposed to be in situ synthesized during the corresponding sol to monolithic xerogel conversion accompanied with the evaporation of HCl, respectively.

The synthesis of the singly Ln^{3+}-ion-doped silica gel (Ln gel; Ln = Nd^{3+}, Yb^{3+}) is similar to that of the Ln−D−P gel except that the $LnCl_3$ ethanol solution was introduced into the starting solution instead of DBM, phen, and $LnCl_3$ ethanol solution. And the concentration of the Ln^{3+} ion is also Ln^{3+}/Si = 1 mol %. The pure gel was synthesized as follows. The molar ratio of tetraethoxysilane (TEOS)/ethanol/deionized water (acidified with HCl) in the starting solution was 1:4:4. The resulting clear sol with a pH value of about 2.5 was stirred for 2 h at RT to ensure homogeneous mixing and complete hydrolysis, and then placed in a sealed plastic container. The precursor solution converted to wet gel after several days of gelation at 40 °C and then was continuously dried to obtain a transparent monolithic gel.

2.4. Equipment and Measurements. All measurements were performed at RT. The elemental analyses of carbon, hydrogen, and nitrogen were carried out on a VarioEL analyzer. FT-IR spectra were measured within a 4000−400 cm^{-1} region on a Bio-Rad model FTS135 infrared spectrophotometer with the KBr pellet technique. The DR measurements were performed on a Hitachi U-4100 spectrophotometer. The UV−vis absorption spectra of DBM and phen were taken with a TU-1901 spectrophotometer using an ethanol solvent. The fluorescence spectra were recorded on an Edinburgh Analytical Instruments FLS920 equipped with the laser diode (LD) from the PicoQuant Company as the light source. The experimental lifetime was measured with a TR550 (J−Y Company) upon excitation with a Nd:YAG laser. The sample gel with a diameter of 5.30 mm and a thickness of 8.92 mm was applied to the optical absorption measurement. The spectral optical density $OD(\lambda) = 0.4343 l\rho\sigma(\lambda)$ of Nd−D−P gel was recorded at room temperature using a Shimadzu UV-3101 PC, where l is the thickness of the Nd−D−P gel, ρ is the concentration of the Nd^{3+} ion in the Nd−D−P gel, and $\sigma(\lambda)$ is the absorption cross section. The corresponding concentration is 7.3×10^{19} Nd/cm^3.

3. Results and Discussion

3.1. Crystal Structures of Nd(DBM)$_3$phen·0.5(C_2H_5OH) and Yb(DBM)$_3$phen Complexes. The crystal structure of Nd(DBM)$_3$phen·0.5(C_2H_5OH) with the numbering scheme is displayed in Figure 1a. Important experimental parameters for the structure determinations are tabulated in Table 1. The central Nd^{3+} ion is coordinated by six oxygen atoms from three DBM ligands and two nitrogen atoms from the phen ligand. Thus, the Nd^{3+} ion exhibits a coordination number of eight. The coordination geometry of the central Nd^{3+} ion may be described as a square antiprism from the coordination site angles (shown in Figure 1b). Crystallization of Yb(DBM)$_3$phen (Figure 2a, Table 1) is of a similar manner. The coordination number of the central Yb^{3+} ion is also eight, yet the polyhedron can be regarded as a dodecahedron (shown in Figure 2b). In the β-diketone rings of two lanthanide complexes, all of the average distances for the carbon−carbon and carbon−oxygen bonds are between the single bond distance and the double bond distance. This can be explained by the fact that there exists conjugated structure between the phenyl ring and the coordinated β-diketonate, which leads to the delocalization of electron density of the coordinated β-diketonate chelate ring. Also, the β-diketonate chelate ring itself is a conjugated structure due to the delocalization of electron density.[15b]

3.2. IR and DR Spectra. The FT-IR spectra of the Nd(DBM)$_3$phen and Yb(DBM)$_3$phen complexes, the Nd−D−P and Yb−D−P gels, and the pure gel are shown in Figure 3. For the Nd(DBM)$_3$phen complex (Figure 3A), both the coordination bonds of Nd−phen and Nd−DBM are evident by the bands appearingin the range of 400−438 cm^{-1}, corresponding to the ν_{Nd-O} vibration and the peak at 511 cm^{-1} due to the ν_{Nd-N} vibration.[16,17] With respect to the IR spectrum of the Nd−D−P gel in Figure 3B, the peak at 1077 cm^{-1} can be attributed to the Si−O−Si symmetric stretching vibration, and the band at

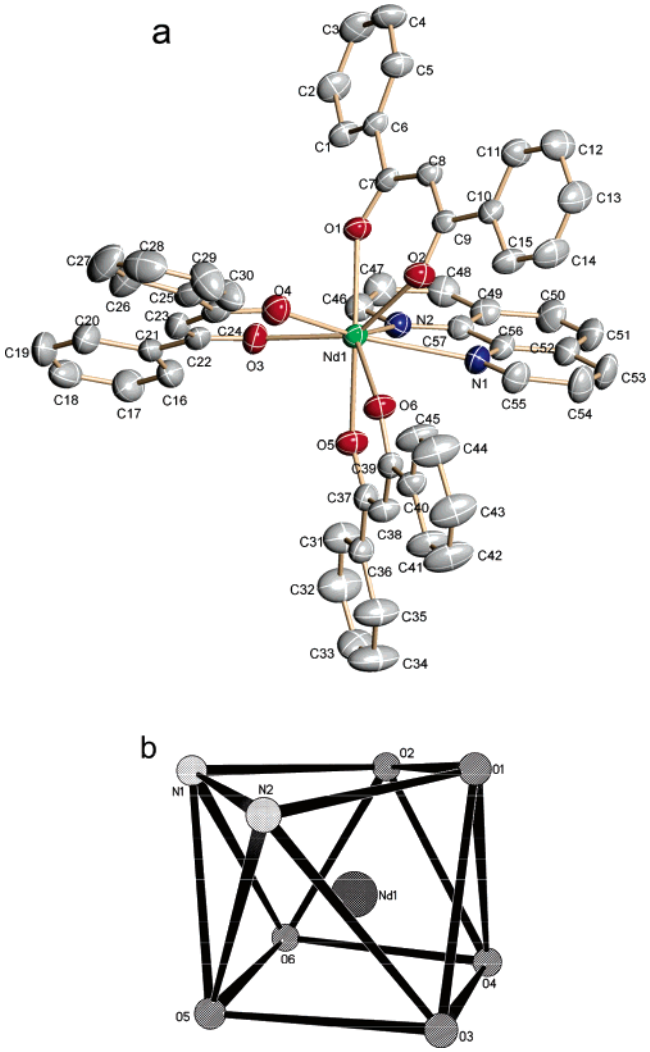

Figure 1. (a) ORTEP plot for $Nd(DBM)_3phen \cdot 0.5(C_2H_5OH)$ with ellipsoids drawn at the 30% probability level. Hydrogen atoms and ethanol were omitted for clarity. (b) Coordination polyhedron of the neodymium (III) ion.

452 cm^{-1} corresponds to the bending vibration of the O−Si−O band.[18] It is worth noting that the stretching vibration frequency of C═N of phen in the Nd−D−P gel has red-shifted to 1620 cm^{-1} compared to pure phen, which can suggest the possible coordination of Nd−N. In comparison to the region 400−457 cm^{-1} of Figure 3E (see inset), in Figure 3B a new absorption band appears at 417 cm^{-1} (see inset) that can be assigned to the stretching band of Nd−O,[17,19] even though it is not prominent. This is probably due to the low concentration of Nd^{3+} ions in the Nd−D−P gel matrix (Ln^{3+}/Si = 1 mol %). For $Yb(DBM)_3phen$ and Yb−D−P gel (Figures 3C and 3D), the IR spectra are similar to those of $Nd(DBM)_3phen$ and Nd−D−P gel, respectively. Therefore, the possible in situ syntheses of lanthanide complexes in the corresponding Ln−D−P gels (Ln = Nd, Yb) can be suggested.

The DR spectra of the $Nd(DBM)_3phen$ complex, Nd−D−P gel, and Nd gel are shown in Figure 4. The band at 1180 nm, which is not shown in the DR spectrum of the $Nd(DBM)_3phen$ complex but shown in the DR spectra of the Nd−D−P gel and the Nd gel, may be assigned to the absorption of the silica gel. In comparison to the DR spectrum of the Nd gel (Figure 4C), in the UV region of curves A and B (200−400 nm) broad absorption bands are both observed and can be attributed to electronic transitions from the ground-state level (π) S_0 to the excited level (π^*) S_1 of the organic ligands. In curves A and B, the characteristic absorption bands due to the transition from the ground state to the excited states of the Nd^{3+} ions are both observed, where the peaks at 514, 527, 581, 675, 747, 802, and 875 nm are assigned to $^4I_{9/2} \rightarrow {}^2G_{11/2}$, $^4I_{9/2} \rightarrow {}^2G_{9/2}$, $^4I_{9/2} \rightarrow {}^2G_{7/2}$, $^4I_{9/2} \rightarrow {}^4F_{9/2}$, $^4I_{9/2} \rightarrow {}^4F_{7/2}$, $^4I_{9/2} \rightarrow {}^4F_{5/2}$, and $^4I_{9/2} \rightarrow {}^4F_{3/2}$, respectively.[20] This, together with the appearance of similar absorption of ligands in both curves, suggests that the neodymium complex is in situ synthesized in the Nd−D−P gel. Similarly, in the DR spectra of the $Yb(DBM)_3phen$ complex and the Yb−D−P gel (Figure 5), the broad ligands absorption bands (200−400 nm) and the characteristic absorption band of the Yb^{3+} ion at 975 nm ($^2F_{9/2} \rightarrow {}^2F_{5/2}$) are both observed, which also suggests that the ytterbium complex is in situ synthesized in the Yb−D−P gel.

TABLE 1: Crystal Data and Structure Refinement for $Nd(DBM)_3phen \cdot 0.5(C_2H_5OH)$ and $Yb(DBM)_3phen$

empirical formula	$C_{58}H_{44}N_2NdO_{6.50}$	$C_{57}H_{41}N_2O_6Yb$
formula weight	1017.19	1022.96
temperature (K)	293(2)	293(2)
wavelength (Å)	0.71073	0.71073
crystal system	triclinic	monoclinic
space group	$P\bar{1}$	$P2_1/n$
a (Å)	12.5701(8)	15.5804(16)
b (Å)	13.0988(8)	17.0282(17)
c (Å)	16.2767(10)	17.6621(18)
α (deg)	93.1700(10)	90
β (deg)	96.4480(10)	91.779(2)
γ (deg)	109.3870(10)	90
volume (Å^3), Z	2499.8(3), 2	4683.6(8), 4
D_{calc} (Mg/m^3)	1.351	1.451
absorption coefficient (mm^{-1})	1.092	2.051
$F(000)$	1036	2060
crystal size (mm)	0.21 × 0.18 × 0.09	0.25 × 0.17 × 0.09
θ range (deg)	1.73 to 26.02	1.66 to 26.18
limiting indices	$-15 \le h \le 12$, $-13 \le k \le 16$, $-20 \le l \le 19$	$-19 \le h \le 19$, $-21 \le k \le 17$, $y-19 \le l \le 21$
reflections collected	14 101	26 141
independent reflections	9582 ($R_{int} = 0.0296$)	9294 ($R_{int} = 0.0248$)
max. and min. transmission	0.9081 and 0.8032	0.8369 and 0.6281
refinement method	full-matrix least squares on F^2	full-matrix least squares on F^2
data/restraints/parameters	9582/2/607	9294/0/595
goodness-of-fit on F^2	1.069	1.033
final R indices ($I > 2\sigma(I)$)	$R_1 = 0.0601$, $wR_2 = 0.1452$	$R_1 = 0.0330$, $wR_2 = 0.0734$
R indices (all data)	$R_1 = 0.0791$, $wR_2 = 0.1580$	$R_1 = 0.0454$, $wR_2 = 0.0798$
largest difference peak and hole (e Å^{-3})	1.424 and −0.422	0.936 and −0.302

3.3. Antenna Fluorescence. The excitation spectra of $Ln(DBM)_3phen$ complexes (Ln = Nd, Yb; monitored at 1060 nm for the $Nd(DBM)_3phen$ complex and 980 nm for the $Yb(DBM)_3phen$ complex) and the absorption spectra of the ligands (DBM and phen) are shown in Figure 6. As is clearly visible in Figure 6, there are overlaps between the excitation band of the lanthanide complexes and the absorption bands of DBM and phen, which indicates the typical sensitization of the Ln^{3+} ions by the two organic ligands, an antenna effect,[9] and thus confirms that the Ln^{3+} ions are surrounded by DBM and phen in the lanthanide complexes.[21] It is also worth noting that the overlap between the absorption of DBM and the lanthanide excitation bands is larger than that between the absorption of phen and the excitation bands, which suggests that the antenna effect of DBM is more efficient than that of phen. Thus, we can come to the conclusion that the intramolecular energy transfer in the $Ln(DBM)_3phen$ complex mainly occurs between the DBM ligand and the Ln^{3+} ions.[15b]

In the excitation spectrum of the $Nd(DBM)_3phen$ complex (Figure 6), a broad band ranging from 230 to 490 nm due to the absorption of the organic ligands superimposed with some

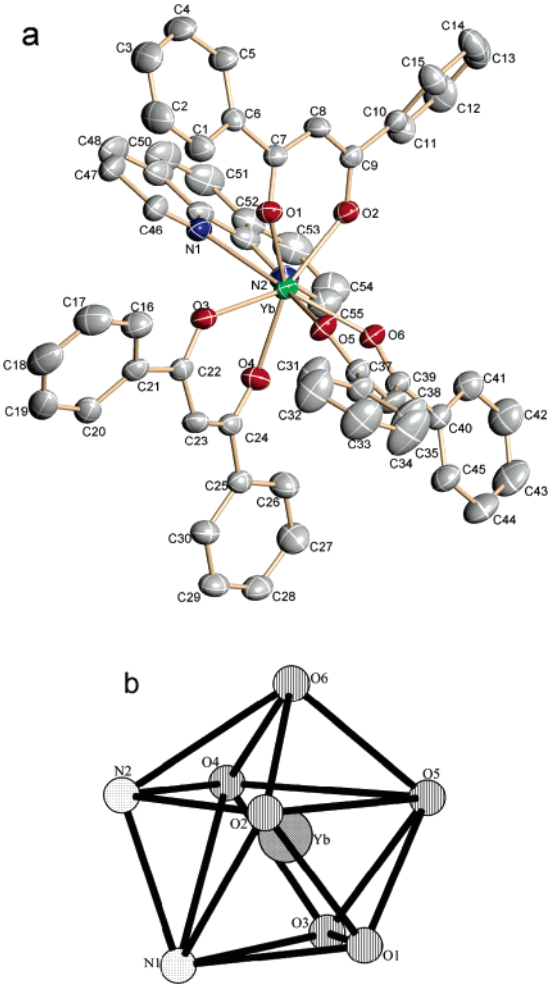

Figure 2. (a) ORTEP plot for Yb(DBM)$_3$phen with ellipsoids drawn at the 30% probability level. Hydrogen atoms were omitted for clarity. (b) Coordination polyhedron of the ytterbium (III) ion.

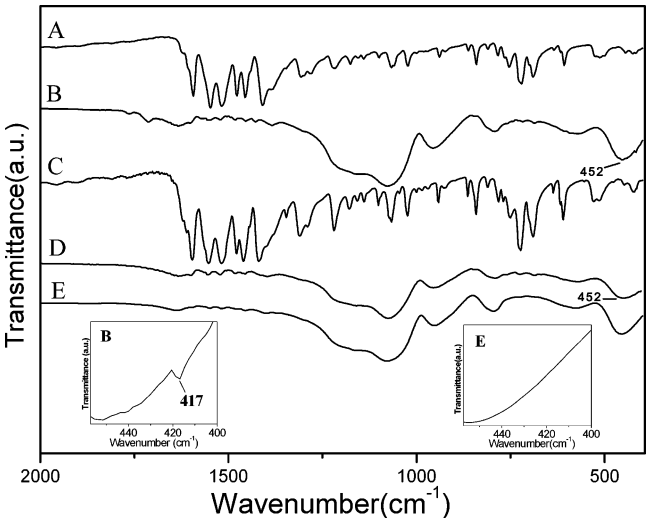

Figure 3. FT-IR spectra of the (A) Nd(DBM)$_3$phen complex, (B) Nd−D−P gel, (C) Yb(DBM)$_3$phen complex, (D) Yb−D−P gel, and (E) pure gel. The inset shows the 400−457 cm^{-1} range of curves B and E.

excitation bands originating from the characteristic absorption transition of the Nd^{3+} ion is observed. These f−f transitions correspond to $^4I_{9/2} \rightarrow {}^2G_{11/2}$ (513 nm) and $^4I_{9/2} \rightarrow {}^2G_{9/2}$ (527 nm) of the Nd^{3+} ion, which are in agreement with those of the DR spectrum (Figure 4A). It is worth noting that these absorption transitions are weaker than those of the ligands,

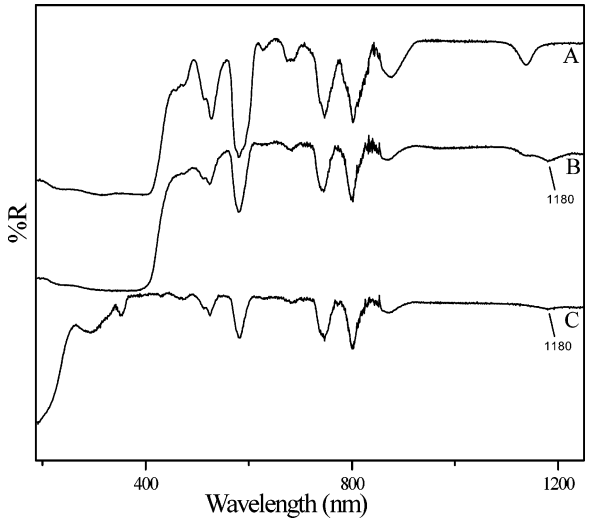

Figure 4. DR spectra of the (A) Nd(DBM)$_3$phen complex, (B) Nd−D−P gel, and (C) Nd gel.

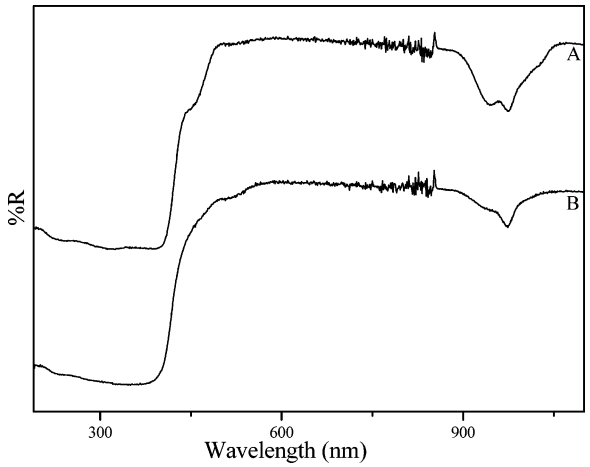

Figure 5. DR spectra of the (A) Yb(DBM)$_3$phen complex and (B) Yb−D−P gel.

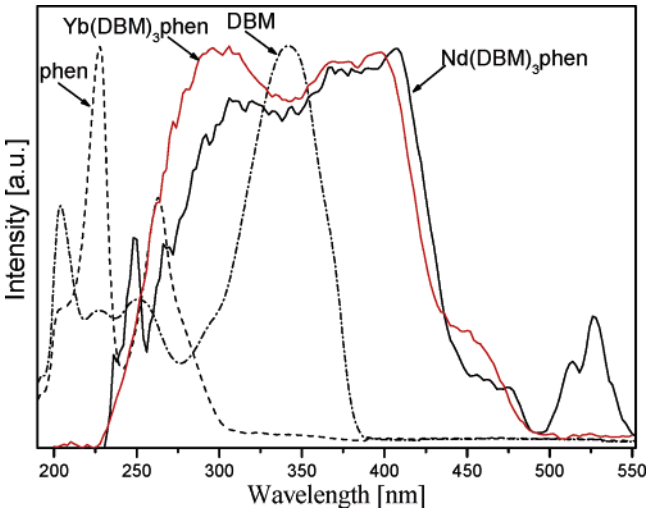

Figure 6. Excitation spectra of Nd(DBM)$_3$phen (λ_{em} = 1060 nm) and Yb(DBM)$_3$phen (λ_{em} = 980 nm) and UV−vis absorption spectra of DBM and phen.

which proves that luminescence sensitization via excitation of ligands is much more efficient than direct excitation of the absorption levels of the Nd^{3+} ions. For the excitation spectrum of the Nd−D−P gel (λ_{em} = 1064 nm), a similar absorption of

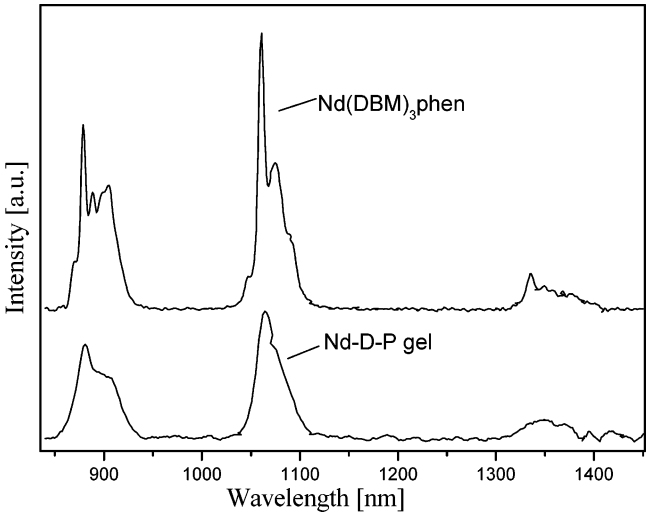

Figure 7. Emission spectra of the $Nd(DBM)_3phen$ complex and Nd−D−P gel (λ_{ex} = 397 nm).

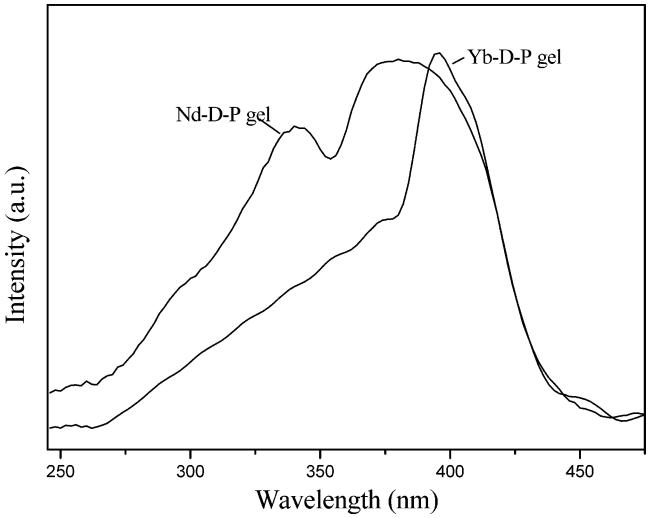

Figure 8. Excitation spectra of the Nd−D−P gel (λ_{em} = 1064 nm) and Yb−D−P gel (λ_{em} = 980 nm).

organic ligands ranging from 250 to 450 nm (Figure 8) is observed compared to that of the $Nd(DBM)_3phen$ complex.

The emission spectra of the $Nd(DBM)_3phen$ complex and the Nd−D−P gel (Figure 7) were obtained upon excitation of the ligands (λ_{ex} = 397 nm). In the two curves, the luminescence spectra of Nd^{III} both consist of three bands at λ = 880, 1060, and 1340 nm, which are attributed to the f−f transitions of $^4F_{3/2}$ (emitting level) → $^4I_{9/2}$, $^4F_{3/2}$ → $^4I_{11/2}$, and $^4F_{3/2}$ → $^4I_{13/2}$, respectively. The strongest emission is observed at 1060 nm, whereas the emissions at 880 and 1340 nm are weaker. The profiles of the emission bands and the relative intensity of the Nd^{3+} luminescence for the $Nd(DBM)_3phen$ complex and the Nd−D−P gel are in agreement with previously reported spectra of organic neodymium complexes.[10,22] To verify that the neodymium complex was in situ synthesized in the Nd−D−P gel, a singly Nd^{3+}-ion-doped silica gel (Nd gel) was prepared using the same Nd/Si molar ratio. In the corresponding emission spectrum (not shown), no characteristic peaks of the Nd^{3+} ion could be detected by excitation at 397 nm in our experimental conditions. The result indicates that in the Nd−D−P gel the obtained characteristic luminescence of the Nd^{3+} ion irradiated at 397 nm is undoubtedly attributable to the contribution of the intramolecular energy transfer from the organic ligands, since the Nd^{3+} ion has no absorption at this wavelength. All of these

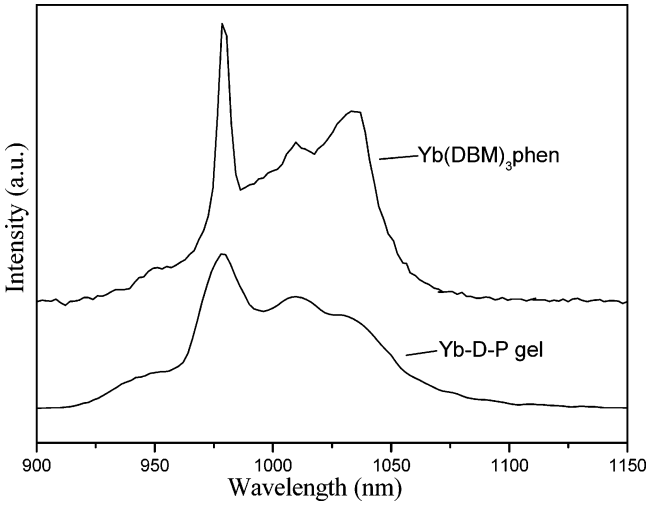

Figure 9. Emission spectra of the $Yb(DBM)_3phen$ complex and Yb−D−P gel (λ_{ex} = 397 nm).

results verify that the neodymium complex is in situ synthesized in the Nd−D−P gel, which is in accord with the preliminary conclusion obtained from the IR and DR spectra.

The excitation spectra of the $Yb(DBM)_3phen$ complex (Figure 6) and the Yb−D−P gel (Figure 8) were obtained by monitoring the characteristic emission of the Yb^{3+} ions at 980 nm. The excitation spectra are dominated by a broad band ranging from 225 to 500 nm for the $Yb(DBM)_3phen$ complex and a broad band from 260 to 466 nm for the Yb−D−P gel. These two broad bands can be assigned to the absorption of the organic ligands and are agreement with those in the DR spectra (Figure 5).

The emission spectra of the $Yb(DBM)_3phen$ complex and the Yb−D−P gel (Figure 9) were obtained by direct excitation of the ligands (λ_{ex} = 397 nm). The emission spectrum of the Yb−D−P gel is similar to that of the $Yb(DBM)_3phen$ complex. In both curves, the prominent 980 nm emission band can be observed, which is assigned to the $^2F_{5/2}$ → $^2F_{7/2}$ transition of the Yb^{3+} ion. It should be noted that the Yb^{3+} ion emission band is not a single sharp transition but an envelope of bands arising at lower and higher energies than the primary 980 nm band. Similar splitting has been reported previously,[22a,23] and in early spectroscopic studies on ytterbium β-diketone compounds it was suggested that crystal field splitting is the origin of the structure in the emission spectra.[24] As discussed for the Nd−D−P gel above, to verify that the ytterbium complex was in situ synthesized in the Yb−D−P gel, a singly Yb^{3+}-ion-doped silica gel (Yb gel) was also prepared with the same Yb/Si molar ratio. In the corresponding emission spectrum (not shown), by excitation at 397 nm no characteristic peak of the Yb^{3+} ion could be detected in our experimental conditions, which indicates that in the Yb−D−P gel the Yb^{3+} ion emission does come from the contribution of the energy transfer from the organic ligands. This confirms that the ytterbium complex is also in situ synthesized in the Yb−D−P gel, which is in agreement with the conclusion obtained from the IR and DR spectra.

3.4. Energy Transfer Mechanism. Direct excitation is very demanding because the optical transitions within the 4f subshells of lanthanide ions are parity forbidden. The indirect excitation by energy transfer from an organic antenna chromophore not only circumvents this excitation problem but also allows excitation at wavelengths where the lanthanide ion does not display a significant absorption. To obtain an excellent luminescent material, one has to take advantage of the strong

SCHEME 1: Model for the Main Pathways in the Sensitization Process (Left) and Energy Diagram of the 4f Levels of the Nd^{3+} and Yb^{3+} Ions (Right)

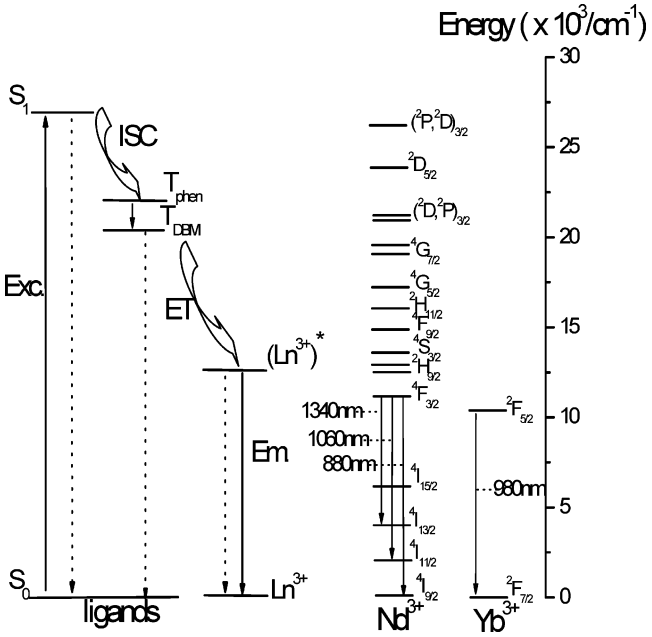

absorbing capacity of organic ligands and the possibility of transferring the excitation energy from the triplet states of the ligands to the lanthanide ions. As described above, we obtained the characteristic Ln^{3+} ion emission upon excitation at the absorption of the organic ligands in both $Ln(DBM)_3$phen complexes and Ln−D−P gels. This indicates that (1) ligands (DBM and phen) are able to transfer the absorbed energy to the central metal Ln^{3+} ions, an antenna effect, which is in agreement with the excitation results mentioned above (Figure 6) and (2) complexes are formed between the Ln^{3+} ions and the ligands. The near-infrared luminescence obtained in this study shows that the ligands shield the lanthanide ions well from their surroundings and efficiently transfer energy from their triplet states to the Ln^{3+} ions. Thus, a model for the indirect excitation mechanism is suggested and shown as a schematic energy diagram in Scheme 1. From the scheme, it can be seen that the electrons of the ligands of the lanthanide complex are excited from the singlet S_0 ground state to the singlet S_1 excited state by absorbing the energy. The energy of the S_1 excited state is then transferred to the triplet excited state of the ligands through intersystem crossing. And subsequently the excitation energy is transferred to the 4f states of the Ln^{3+} ions, ultimately resulting in sensitized Ln^{3+} ion emission.[25]

A detailed scheme of the 4f energy levels of the Nd^{3+} and Yb^{3+} ions is depicted on the right of Scheme 1. As discussed above, for the $Nd(DBM)_3$phen complex and the Nd−D−P gel (Figure 7), the emission bands at 880, 1060, and 1340 nm correspond to the $^4F_{3/2} \rightarrow {}^4I_{9/2}$, $^4F_{3/2} \rightarrow {}^4I_{11/2}$, and $^4F_{3/2} \rightarrow {}^4I_{13/2}$ transitions, respectively. That is to say that through intramolecular energy transfer process the excitation energy is transferred from the ligands to the 4f levels of the Nd^{3+} ion. And from the upper 4f levels, the relaxation to the $^4F_{3/2}$ first excited state of Nd^{3+} can take place, and finally the Nd^{3+} ion may decay to the $^4I_{9/2}$, $^4I_{11/2}$, and $^4I_{13/2}$ states by the emissions of 880, 1060, and 1340 nm, respectively. Among the three emission bands, the band at 1060 nm is the most important because it is potentially applicable for laser emission.[26] For the $Yb(DBM)_3$-phen complex and the Yb−D−P gel, the Yb^{3+} ion has some advantages for laser emission due to its very simple energy level scheme (the right of Scheme 1), consisting of only two levels, the $^2F_{7/2}$ ground state and the $^2F_{5/2}$ excited state. There is no excited-state absorption upon reducing the effective laser cross section, no up-conversion, no concentration quenching, and no absorption in the visible range.[27] As discussed above, the obtained characteristic band at 980 nm is assigned to the $^2F_{5/2} \rightarrow {}^2F_{7/2}$ transition of the Yb^{3+} ion in the $Yb(DBM)_3$phen complex and the Yb−D−P gel (Figure 9), which is also very important for laser emission.

Lanthanides that emit at longer wavelengths have relatively small energy gaps between the excited and the ground state. This allows the use of antenna with much lower triplet state energies.[4a] For energy transfer to occur efficiently, there should be spectral overlap between the donor (ligand) and the acceptor (Ln^{3+} ion) states. According to Dexter's theory,[28] the suitability of the energy difference between the resonance level of the Ln^{3+} ion and the triplet state of the ligand is a critical factor for efficient energy transfer. If the energy difference is too big, then the energy transfer rate constant will decrease due to the diminution in the overlap between the donor and the acceptor. On the contrary, if the energy difference is too small, then the energy back-transfer can occur from the Ln^{3+} ion to the resonance level of the triplet state of the ligand. The energy gap must be at least $10k_BT$, (2000 cm^{-1}) to effectively preclude energy back-transfer.[29] DBM, whose triplet state is 20 400 cm^{-1},[30] can match well with the 4f levels of the Nd^{3+} and Yb^{3+} ions. In the meantime, using the β-diketonate as a ligand for neodymium and ytterbium in the matrix has several advantages. First, the ligand protects the Ln^{3+} ions (Ln = Nd, Yb) from the residual water molecules and silanol groups in the sol−gel matrix, which decreases the quenching effect due to the high energy vibration of the water molecules. Second, the diketonate ligand has a long wavelength absorption for its $\pi-\pi^*$ transition and consequently has been targeted for its ability to sensitize the luminescence of the Ln^{3+} ions at relatively long wavelengths. Third, since the coordination ability of oxygen with the lanthanide ions is stronger than that of nitrogen, in the absence of β-diketonate, the phen ligand cannot successfully compete with the water molecules for a place in the first coordination sphere around the lanthanide ions.[31] Phen, which is widely used as the second ligand in the complexes, was introduced in our lanthanide complexes to better sensitize Ln^{3+} ion luminescence by replacing the H_2O groups that can quench the luminescence of the Ln^{3+} ions and optimizing the emission intensity of the Ln^{3+} ions. The combination of both ligands has essentially complementary absorption spectra in the UV region and effectively sensitizes over a wide wavelength range followed by transferring the energy to the central Ln^{3+} ions.

3.5. Judd−Ofelt Analysis. It is known that the Judd−Ofelt theory[14] is one of the most successful theories in estimating the magnitude of the forced electric dipole transitions of rare earth ions. As discussed above, the Nd−D−P gel has the potential for development in laser applications. To further evaluate the potential of rare-earth-doped materials, it is essential to study the radiative properties of the rare earth organic complexes. As usual, the radiative properties of trivalent rare earth ions in host matrix can be predicted from optical absorption measurements and by using the Judd−Ofelt theory.

According to the Judd−Ofelt theory, the data of the absorption spectrum can be used to predict the radiative lifetime of the Nd^{3+} ion $^4F_{3/2}$ excited J manifold and the branching rations of the fluorescence transitions to the lower-lying ^4I_J manifold. The procedure involves first measuring the line oscillator strength S_{exp} of the transitions between the ground $^4I_{9/2}$ J

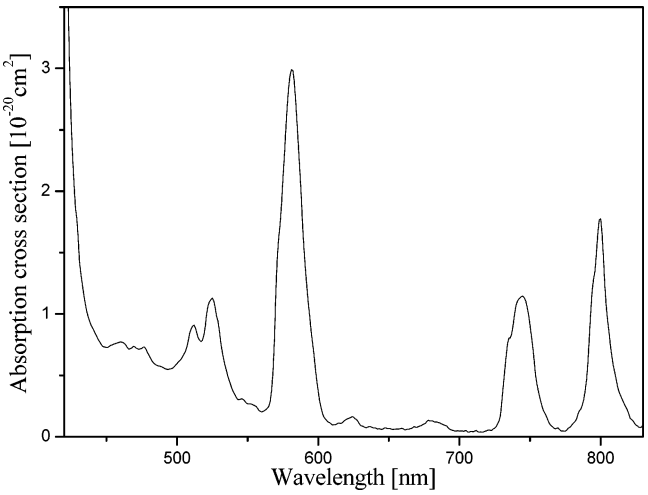

Figure 10. Absorption spectrum of the Nd−D−P gel.

TABLE 2: Measured and Calculated Line Strengths of the Nd^{3+} Ion in the Nd−D−P Gel[a]

level	λ (nm)	S_{exp} ($\times 10^{-20}$ cm^2)	S_{cal} ($\times 10^{-20}$ cm^2)
$^2G_{7/2}$	581	6.7508	6.7500
$^2H_{11/2}$	624	0.0680	0.0524
$^4F_{9/2}$	681.5	0.1607	0.2403
$^4S_{3/2}$	742.6	2.3157	2.3119
$^4F_{7/2}$			
$^4F_{5/2}$	799.1	2.4270	2.4254

[a] All transitions are from the $^4I_{9/2}$ state.

manifold and the excited J manifolds of the Nd^{3+} ion. Figure 10 shows the absorption spectrum of the Nd−D−P gel. Five Nd^{3+} ion absorption bands in the absorption spectrum were selected to determine the phenomenological oscillator strength parameters. The band positions along with the assignments in the absorption spectrum are shown in Table 2. The measured line strength S_{mea} can be determined using the following expression[32]

$$\int \sigma(\lambda)\, d\lambda = \frac{8\pi^3 e^2 \bar{\lambda}}{3ch(2J+1)} \frac{1}{n}\left[\frac{(n^2+2)^2}{9}\right] S_{exp} \qquad (1)$$

where $\sigma(\lambda)$ is the absorption cross section at wavelength λ, $\bar{\lambda}$ is the mean wavelength of the specific absorption band, e, h, and c are the electron charge, Planck's constant, and the velocity of light, respectively. J is the total angular momentum quantum number of the initial level (for Nd^{3+} ion $J = {}^9/_2$). And an average index of refraction of 1.5 was used.[33]

According to Judd−Ofelt theory,[14] the experimental oscillator strength of an electric dipole transition between an initial J manifold $|(S,L)J\rangle$ and a terminal J' manifold $|(S',L')J'\rangle$ can be expressed as the form[34]

$$S = \sum_{t=2,4,6} \Omega_t |\langle (S,L)J \| U^{(t)} \| (S',L')J' \rangle|^2 \qquad (2)$$

where $\langle \| U^{(t)} \| \rangle$ are the doubly reduced matrix elements corresponding to the $J-J'$ transition. The matrix elements depend only on the angular momentum of the Nd^{3+} ion states and are essentially independent of the ion environment.[35] In our work, the calculated values of the square of the reduced matrix elements are cited from Carnall's data.[36] When two or more absorption manifolds overlapped, the matrix element was taken to be the sum of the corresponding squared matrix elements.[37] The Ω_t ($t = 2, 4, 6$), the oscillator strength parameters, are independent of electronic quantum numbers with the ground $4f^3$ configuration of the Nd^{3+} ion. They may be regarded as phenomenological parameters that characterize the radiative transition probabilities within the ground configuration. Through the use of eq 1, the experimental oscillator strength S_{exp} for the electric dipole transition can be obtained. Then, the parameters Ω_t can be derived by a least-squares fitting of eq 2: $\Omega_2 = 76.23 \times 10^{-20}$ cm^2, $\Omega_4 = 4.778 \times 10^{-20}$ cm^2, $\Omega_6 = 3.064 \times 10^{-20}$ cm^2.

The interpretation of the physical meaning of the phenomenological oscillator strength parameters still remains a controversial matter for discussion. Ω_2 is usually related to the degree of covalency in the lanthanide−first coordination shell interaction.[33b,38] In the sense of the dynamic coupling contribution to the total intensity,[38c] the polarization of the ligand field induces stronger lanthanide−ligand bonds and an increase in electric dipolar transitions for noncentrosymmetric ligand fields. The large value for Ω_2 in this title indicates the presence of covalent bonding between the Nd^{3+} ion and the surrounding ligands, as is reasonable.[35]

The values of the parameters are then used to recalculate the transition line strengths of the absorption bands using eq 2. The calculated line strengths S_{cal} of the five absorption bands are tabulated in Table 2. To justify the results obtained, a measure of the accuracy of the fit is given by the root-mean-square (rms) deviation of the experimental and calculated line strengths, which is obtained by

$$\mathrm{rms}\Delta S = \left[\frac{(S_{mea} - S_{cal})^2}{N - M}\right]^{1/2} \qquad (3)$$

where N is the number of spectral bands analyzed and M is the number of parameters determined. In this case, $M = 3$. The values in Table 2 provide an rms deviation of 0.0574×10^{-20} cm^2, which indicates that the result derived by a least-squares fitting of eq 2 is good.

From the parameters Ω_t obtained above, the radiative transition rates for electric dipole transitions from the initial J' manifold $|(S',L')J'\rangle$ to the terminal manifold $|(\bar{S},\bar{L})\bar{J}\rangle$ can be calculated using the following expression[30]

$$A[^4F_{3/2};(\bar{S},\bar{L})\bar{J}] = \frac{64\pi^4 e^2}{3h(2J'+1)\bar{\lambda}^3} \frac{n(n^2+2)^2}{9} \times \sum_{t=2,4,6} \Omega_t |\langle {}^4F_{3/2} \| U^{(t)} \| (\bar{S},\bar{L})\bar{J} \rangle|^2 \qquad (4)$$

where $(\bar{S},\bar{L})\bar{J}$ are quantum numbers of the lower states, $J' = {}^3/_2$, and $\bar{\lambda}$ is the mean wavelength of the emission transition (Figure 7). And the related reduced matrix elements of the emissive transitions are given in ref 39 for the Nd^{3+} ion.

The radiative lifetime represents an effective average over site-to-site variations in the local Nd^{3+} environment. The radiative lifetime (τ_{rad}) and the total radiative transition rate are related by the expression[40]

$$\tau_{rad} = \frac{1}{\sum_{\bar{S},\bar{L},\bar{J}} A[(S',L')J';(\bar{S},\bar{L})\bar{J}]} \qquad (5)$$

And the fluorescence branching ratios can be determined from the radiative decay rates by

$$\beta[(S',L')J';(\bar{S},\bar{L})\bar{J}] = \frac{A[(S',L')J';(\bar{S},\bar{L})\bar{J}]}{\sum_{\bar{S},\bar{L},\bar{J}} A[(S',L')J';(\bar{S},\bar{L})\bar{J}]} \quad (6)$$

The radiative lifetime of the $^4F_{3/2}$ state has been calculated to be 523 μs, which is an important parameter in consideration of the pumping requirement for the threshold of laser action.[41] The experimental lifetime of the $^4F_{3/2}$ state was measured. Analysis of the monoexponential decay results in a lifetime of 54 μs, which is lower than the radiative lifetime calculated from the theory. This is due to the effect of the radiationless relaxation process, which results in the difference between the experimental lifetime and the calculated result. Work on decreasing the effect of the radiationless relaxation is in process. The fluorescence branching ratio is a critical parameter to the laser designer, because it characterizes the possibility of attaining stimulated emission from any specific transition.[42]

With the value for the radiative transition rate calculated above and the corresponding emission spectrum, for a Lorentz line the stimulated emission cross section σ_e is calculated by

$$\sigma_e = \frac{A\lambda^2}{4\pi^2 n^2 \Delta\nu} \quad (7)$$

where $\Delta\nu$ is the frequency full width at half-maximum and λ is the wavelength of the emission peak. The values of the radiative transition rates A, the fluorescence branching ratios β, the radiative lifetime τ_{rad}, and the emission cross section σ_e are presented in Table 3.

It can be shown that the radiative lifetime of the transition involved is comparable with the radiative lifetimes of neodymium laser glasses.[43] The emission cross section σ_e of the $^4F_{3/2} \rightarrow {}^4I_{11/2}$ fluorescence transition of the Nd^{3+} ion is one of the most important parameters for laser design, and it is dependent only on Ω_4 and Ω_6, because of the triangle rule $|J - J'| \leq \lambda \leq (J + J')$, $||U^{(t)}||^2 = 0$ $(t = 2)$.[39] In our case, the stimulated emission cross section of the $^4F_{3/2} \rightarrow {}^4I_{11/2}$ fluorescence transition of the Nd^{3+} ion in the Nd−D−P gel is 1.414×10^{-20} cm^2, which is comparable with those shown by glasses used in solid-state laser applications.[44] All of these showed that the $^4F_{3/2} \rightarrow {}^4I_{11/2}$ transition of the Nd^{3+} ion in the Nd−D−P gel can be considered as a possible laser transition.

4. Conclusions

We successfully demonstrated the crystal structures of the $Ln(DBM)_3$phen complexes and the syntheses of transparent homogeneous hybrid materials containing the corresponding lanthanide complex by using an in situ synthesis technique. The properties of the Ln−D−P gel were investigated and compared with those of the $Ln(DBM)_3$phen complexes. The evidence for the lanthanide complex in situ synthesized in the corresponding Ln−D−P gel was mainly obtained from fluorescence properties. We have demonstrated the NIR luminescence of $Ln(DBM)_3$phen complexes and Ln−D−P gels upon indirect excitation of them, mediated by the sensitizing effect of the ligands in the lanthanide complexes, an antenna effect. According to the Judd−Ofelt theory, the radiative properties of the Nd^{3+} ion in the Nd−D−P gel, such as radiative transition rates, emission cross sections, fluorescence branching ratios, and radiative lifetime were calculated and analyzed. On the basis of the experimental data and Judd−Ofelt analysis, we can come to the conclusion that the $^4F_{3/2} \rightarrow {}^4I_{11/2}$ transition of the Nd^{3+} ion in the Nd−D−P gel can be considered as a possible candidate for a solid-state laser transition.

TABLE 3: Spectra Parameters for the $^4F_{3/2} \rightarrow {}^4I_J$ Transition of the Nd^{3+} Ion in the Nd−D−P Gel

$^4F_{3/2} \rightarrow (S',L')J'$	λ (nm)	S_{cal} ($\times 10^{-20}$ cm^2)	A (s^{-1})	β_c	σ_e ($\times 10^{-20}$ cm^2)
$^4F_{3/2} \rightarrow {}^4I_{9/2}$	881	1.263	969.1	0.507	0.511
$^4F_{3/2} \rightarrow {}^4I_{11/2}$	1064	1.800	802.4	0.420	1.414
$^4F_{3/2} \rightarrow {}^4I_{13/2}$	1349	0.639	140.8	0.073	0.320
τ_{rad} (μs)		523			

Acknowledgment. This work was supported by the National Natural Science Foundation of China (Grant Nos. 20171043 and 20372060), the Key National Natural Science Foundation of China (Grant No. 20131010), the National Natural Science Foundation of China—Special for Instruments (Grant No. 20121701), the "863" National Foundation for High Technology Development and Programming (Grant No. 2002AA302105_2002AA324080), and the Foreign Communion & Cooperation of the National Natural Science Foundation of China (Grant No. 20340420326). We are grateful to Professor Jiang-Gao Mao of the Fujian Institute of Research on the Structure of Matter, Chinese Academy of Sciences for assistance with the fluorescence measurements. We also thank Professors Si-Yuan Zhang and Zhi-Jian Wu of the Changchun Institute of Applied Chemistry guidance with the Judd−Ofelt theory.

Supporting Information Available: Crystallographic information for $Nd(DBM)_3phen{\cdot}0.5(C_2H_5OH)$ and $Yb(DBM)_3phen$. This material is available free of charge via the Internet at http://pubs.acs.org.

References and Notes

(1) Sabbatini, N.; Guardigli, M.; Lehn, J.-M. *Coord. Chem. Rev.* **1993**, *123*, 201.

(2) (a) Parker, D.; Williams, J. A. G. *J. Chem. Soc., Dalton Trans.* **1996**, 3613. (b) Elbanowski, M.; Makowska, B. *J. Photochem. Photobiol., A* **1996**, *99*, 85. (c) Sabbatini, N.; Guardigli, M.; Manet, I. *Adv. Photochem.* **1997**, *23*, 213.

(3) (a) Beeby, A.; Faulkner, S. *Chem. Phys. Lett.*, **1997**, *266*, 116. (b) Imbert, D.; Cantuel, M.; Bünzli, J. C. G.; Bernardinelli, G.; Piguet, C. *J. Am. Chem. Soc.* **2003**, *125*, 15698.

(4) (a) Beeby, A.; Dickins, R. S.; Faulkner, S.; Parker, D.; Williams, J. A. G. *Chem. Commun.* **1997**, 1401. (b) Horrocks, W. D., Jr.; Bolender, J. P.; Smith, W. D.; Supkowski, R. M. *J. Am. Chem. Soc.* **1997**, *119*, 5972. (c) Kang, T. S.; Harrison, B. S.; Bouguettaya, M.; Foley, T. J.; Boncella, J. M.; Schanze, K. S.; Reynolds, J. R. *Adv. Funct. Mater.* **2003**, *13*, 205.

(5) (a) Weber, M. J. In *Lanthanide and Actinide Chemistry and Spectroscopy*; Edelstein, N. M., Ed.; ACS Symposium Series 131; American Chemical Society: Washington, DC, 1980, p 275. (b) Ryo, M.; Wada, Y.; Okubo, T.; Hasegawa, Y.; Yanagida, S. *J. Phys. Chem. B* **2003,** *107*, 11302.

(6) Davies, G. M.; Aarons, R. J.; Motson, G. R.; Jeffery, J. C.; Adams, H.; Faulkner, S.; Ward, M. D. *J. Chem. Soc., Dalton Trans.* **2004**, 1136.

(7) Weissman, S. I. *J. Chem. Phys.* **1942**, *10*, 214.

(8) (a) Melby, L. R.; Rose, N. J.; Abramson, E.; Caris, J. C. *J. Am. Chem. Soc.* **1964**, *86*, 5117. (b) Binnemans, K.; Lenaerts, P.; Driesen, K.; Görller-Walrand, C. *J. Mater. Chem.* **2004**, *14*, 191. (c) Carlos, L. D.; Sá Ferreira, R. A.; Rainho, J. P.; de Zea Bermudez, V. *Adv. Funct. Mater.* **2002**, *12*, 819.

(9) (a) Bekiari, V.; Lianos, P. *Adv. Mater.* **1998**, *10*, 1455. (b) Sabbatini, N.; Mecati, A.; Guardigli, M.; Balazani, V.; Lehn, J. M.; Zeissel, R.; Ungaro, R. *J. Lumin.* **1991**, *48−49*, 463. (c) Sabbatini, N.; Guardigli, M.; Lehn, J. M. *Coord. Chem. Rev.* **1993**, *123*, 201. (d) Driesen, K.; Deun, R. V.; Görller-Walrand, C.; Binnemans, K. *Chem. Mater.* **2004**, *16*, 1531.

(10) Klink, S. I.; Grave, L.; Reinhoudt, D. N.; van Veggel, F. C. J. M.; Werts, M. H. V.; Geurts, F. A. J.; Hofstraat, J. W. *J. Phys. Chem. A* **2000**, *104*, 5457.

(11) (a) Sanchez, C.; Soler-Illia, G. J. A. A.; Ribot, F.; Lalot, T.; Mayer, C. R.; Cabuil, V. *Chem. Mater.* **2001**, *13*, 3061. (b) Corriu, R. J. P.; Embert, F.; Guari, Y.; Mehdi, A.; Reyé, C. *Chem. Commun.* **2001**, 1116. (c) Hernandez, R.; Franville, A. C.; Minoofar, P.; Dunn, B.; Zink, J. I. *J. Am. Chem. Soc.* **2001**, *123*, 1248. (d) Li, H. H.; Inoue, S.; Machida, K. I.; Adachi, G. Y. *Chem. Mater.* **1999**, *11*, 3171.

(12) (a) Driesen, K.; Görller-Walrand, C.; Binnemans, K. *J. Mater. Sci. Eng. C* **2001**, *18*, 255. (b) Driesen, K.; Lenaerts, P.; Binnemans, K.; Görller-Walrand, C. *Phys. Chem. Chem. Phys.* **2002**, *4*, 552.

(13) (a) Qian, G. D.; Yang, Z.; Wang, M. Q. *J. Lumin.* **2002**, *96*, 211. (b) Qian, G. D.; Wang, M. Q.; Yang, Z. *J. Phys. Chem. Solids* **2002**, *63*, 1829.

(14) (a) Judd, B. R. *Phys. Rev.* **1962**, *127*, 750. (b) Oflet, G. S. *J. Chem. Phys.* **1962**, *37*, 511.

(15) (a) Crystallographic data for the structure reported in this paper have been deposited with the Cambridge Crystallographic Data Centre as supplementary publication no. CCDC-249292 for $Nd(DBM)_3phen \cdot 0.5(C_2H_5OH)$ and CCDC-249293 for $Yb(DBM)_3phen$. Copies of the data can be obtained free of charge via www.ccdc.cam.ac.uk/conts/retrieving.html or on application to The Director, CCDC, 12 Union Road, Cambridge CB2 1EZ, U. K.; fax, (+44) 1223 336 033; e-mail, deposit@ccdc.cam.ac.uk. (b) Yu, J. B.; Zhang, H. J.; Fu, L. S.; Deng, R. P.; Zhou, L.; Li, H. R.; Liu, F. Y.; Fu, H. L. *Inorg. Chem. Commun.* **2003**, *6*, 852.

(16) Bian, L. J.; Xi, H. A.; Qian, X. F.; Yin, J.; Zhu, Z. K.; Lu, Q. H. *Mater. Res. Bull.* **2002**, *37*, 2293.

(17) Li, Y. Y.; Gong, M. L.; Yang, Y. S.; Li, M. Q.; Chen, R. Y. *J. Inorg. Chem.* **1990**, *6*, 249.

(18) Li, H. R.; Zhang, H. J.; Lin, J.; Wang, S. B.; Yang, K. Y. *J. Non-Cryst. Solids* **2000**, *278*, 218.

(19) Holtzclaw, H. F., Jr.; Collman, J. P. *J. Am. Chem. Soc.* **1957**, *79*, 3318.

(20) Hasegawa, Y.; Kimura, Y.; Murakoshi, K.; Wada, Y.; Kim, J. H.; Nakashima, N.; Yamanaka, T.; Yanagida, S. *J. Phys. Chem.* **1996**, *100*, 10201.

(21) (a) Li, H. R.; Lin, J.; Zhang, H. J.; Fu, L. S.; Meng, Q. G.; Wang, S. B. *Chem. Mater.* **2002**, *14*, 3651. (b) Kawa, M.; Fréchet, J. M. J. *Chem. Mater.* **1998**, *10*, 286.

(22) (a) Deun, R. V.; Moors, D.; Fré, B. D.; Binnemans, K. *J. Mater. Chem.* **2003**, *13*, 1520. (b) Iwamuro, M.; Wada, Y.; Kitamura, T.; Nakashima, N.; Yanagida, S. *Phys. Chem. Chem. Phys.* **2000**, *2*, 2291.

(23) (a) Asano-Someda, M.; Kaizu, Y. *J. Photochem. Photobiol., A* **2001**, *139*, 161. (b) Tsvirko, M. P.; Stelmakh, G. F.; Pyatosin, V. E.; Solovyov, K. N.; Kachura, T. F. *Chem. Phys. Lett.* **1980**, *73*, 80.

(24) Perkins, W. G.; Crosby, G. A. *J. Chem. Phys.* **1965**, *42*, 407.

(25) Klink, S. I.; Hebbink, G. A.; Grave, L.; van Veggel, F. C. J. M.; Reinhoudt, D. N.; Slooff, L. H.; Polman, A.; Hofstraat, J. W. *J. Appl. Phys.* **1999**, *86*, 1181.

(26) Klink, S. I.; Alink, P. O.; Grave, L.; Peters, F. G. A.; Hofstraat, J. W.; Geurts, F.; van Veggel, F. C. J. M. *J. Chem. Soc., Perkin Trans. 2* **2001**, 363.

(27) Boulon, G.; Collombet, A.; Brenier, A.; Cohen-Adad, M. T.; Yoshikawa, A.; Lebbou, K.; Lee, J. H.; Fukuda, T. *Adv. Funct. Mater.* **2001**, *11*, 263.

(28) Dexter, D. L. *J. Chem. Phys.* **1953**, *21*, 836.

(29) Beeby, A.; Faulkner, S.; Parker, D.; Williams, J. A. G. *J. Chem. Soc., Perkin Trans. 2* **2001**, 1268.

(30) Kim, H. J.; Lee, J. E.; Kim, Y. S.; Park, N. G. *Opt. Mater.* **2002**, *21*, 181.

(31) (a) Frey, S. T.; Gong, M. L.; Horrocks, W. D., Jr. *Inorg. Chem.* **1994**, *33*, 3229. (b) Frey, S. T.; Horrocks, W. D., Jr. *Inorg. Chim. Acta* **1995**, *229*, 383. (c) Malta, O. L.; Batista, H. J.; Carlos, L. D. *Chem. Phys.* **2002**, *282*, 21.

(32) (a) Wang, G. F.; Chen, W. Z.; Li, Z. B.; Hu, Z. S. *Phys. Rev. B* **1999**, *60*, 15469. (b) Hasegawa, Y.; Yamamuro, M.; Wada, Y.; Kanehisa, N.; Kai, Y.; Yanagida, S. *J. Phys. Chem. A* **2003**, *107*, 1697.

(33) (a) Soares-Santos, P. C. R.; Nogueira, H. I. S.; Félix, V.; Drew, M. G. B.; Sá Ferreira, R. A.; Carlos, L. D.; Trindade, T. *Chem. Mater.* **2003**, *15*, 100. (b) Malta, O. L.; Couto dos Santos, M. A.; Thompson, L. C.; Ito, N. K. *J. Lumin.* **1996**, *69*, 77.

(34) (a) Wang, G. F. *J. Opt. Soc. Am. B* **2001**, *18*, 173. (b) Zheng, Z. Q.; Liang, H.; Ming, H.; Zhang, Q. J.; Xie, J. P. *Opt. Commun.* **2004**, *233*, 149.

(35) Koeppen, C.; Yamada, S.; Jiang, G.; Garito, A. F. *J. Opt. Soc. Am. B* **1997**, *14*, 155.

(36) Carnall, W. T.; Fields, P. R.; Rajnak, K. *J. Chem. Phys.* **1968**, *49*, 4424.

(37) Mehta, V.; Aka, G.; Dawar, A. L.; Mansingh, A. *Opt. Mater.* **1999**, *12*, 53.

(38) (a) Malta, O. L.; Brito, H. F.; Menezes, J. F. S.; Goncalves e Silva, F. R.; Alves, S., Jr.; Farias, F. S., Jr.; de Andrade, A. V. M. *J. Lumin.* **1997**, *75*, 255. (b) Oomen, E. W. J. L.; van Dongen, A. M. A. *J. Non-Cryst. Solids* **1989**, *111*, 205. (c) Judd, B. R. *J. Chem. Phys.* **1979**, *70*, 4830.

(39) Kaminskii, A. A.; Boulon, G.; Buoncristiani, M.; Di Bartolo, B.; Kornienko, A.; Mironov, V. *Phys. Status Solidi A* **1994**, *141*, 471.

(40) Kumar, G. A.; Martinez, A.; Rosa, E. D. L. *J. Lumin.* **2002**, *99*, 141.

(41) Chen, B.; Dong, N.; Zhang, Q. J.; Yin, M.; Xu, J.; Liang, H.; Zhao, H. *J. Non-Cryst. Solids* **2004**, *341*, 53.

(42) Jiang, H. D.; Wang, J. Y.; Zhang, H. J.; Hu, X. B.; Liu, H. *J. Appl. Phys.* **2002**, *92*, 3647.

(43) (a) Speghini, A.; Peruffo, M.; Casarin, M.; Ajò, D.; Bettinelli, M. *J. Alloys Compd.* **2000**, *300*−*301*, 174. (b) Rolli, R.; Gatterer, K.; Wachtler, M.; Bettinelli, M.; Speghini, A.; Ajo, D. *Spectrochim. Acta A* **2001**, *57*, 2009.

(44) Brown, D. C. In *High-Peak-Power Nd:Glass Laser Systems*; Springer Series in Optical Science 25; Springer: Berlin, 1981.